ATMOSPHERIC AEROSOLS

Multiphase buffer theory explains contrasts in atmospheric aerosol acidity

Guangjie Zheng[1], Hang Su[2]*, Siwen Wang[2], Meinrat O. Andreae[2,3,4], Ulrich Pöschl[2], Yafang Cheng[1]*

Aerosol acidity largely regulates the chemistry of atmospheric particles, and resolving the drivers of aerosol pH is key to understanding their environmental effects. We find that an individual buffering agent can adopt different buffer pH values in aerosols and that aerosol pH levels in populated continental regions are widely buffered by the conjugate acid-base pair NH_4^+/NH_3 (ammonium/ammonia). We propose a multiphase buffer theory to explain these large shifts of buffer pH, and we show that aerosol water content and mass concentration play a more important role in determining aerosol pH in ammonia-buffered regions than variations in particle chemical composition. Our results imply that aerosol pH and atmospheric multiphase chemistry are strongly affected by the pervasive human influence on ammonia emissions and the nitrogen cycle in the Anthropocene.

Aerosol acidity has attracted increasing interest in atmospheric research because it influences the thermodynamics of gas-particle partitioning and the chemical kinetics of the formation and transformation of air particulate matter (*1*–*8*). Understanding the temporal and spatial variations of aerosol pH in the atmosphere is crucial for accurate predictions of the properties of atmospheric aerosols and their effects on health, ecosystems, and climate (*9*–*12*). In marine environments, the uptake of acidic gases like SO_2, H_2SO_4, and HNO_3 may rapidly consume the alkalinity and reduce the pH of sea salt aerosols (*13*, *14*). For continental air masses in the southeastern United States, Weber *et al.* (*15*) have suggested that aerosol pH is buffered in the range of ~0 to 2 because of the interaction of aqueous $(NH_4)_2SO_4$-NH_4HSO_4 with gaseous NH_3. However, their later studies have attributed the elevated pH levels in northern China (~3 to 6) (*8*, *16*–*19*) mainly to changes in particle chemical compositions—i.e., a shift from sulfate- to nitrate-dominated aerosols (*12*, *19*)—whereas Cheng *et al.* (*8*) have highlighted the role of ammonia and alkaline aerosol components from natural and anthropogenic emissions in understanding aerosol pH in this region.

Despite these advances, it is still unclear how aerosol pH is buffered in other continental regions, such as northern China, compared with the southeastern United States. To answer this question, we first performed numerical model calculations with the state-of-the-art thermodynamic model ISORROPIA (*20*) to examine the response of pH in aerosols upon the addition of sulfuric acid under different conditions that are characteristic of the southeastern United States (*15*, *21*), the North China Plain (*8*, *22*), northern India (*23*), and western Europe (*24*) [table S1 and (*25*)]. For reference, we also calculated the response of an aqueous solution of Na_2SO_4. As shown in fig. S1, the Na_2SO_4 solution exhibits the expected steep decrease of pH upon acid addition. For aerosol systems, however, the pH does not show a substantial decrease until the added amount of acid (H^+ equivalent) reaches ~20% of the initial amount of anions in the aqueous particles (molar ratio), which indicates an additional buffering effect. To further investigate this phenomenon, we focus on the scenarios for the southeastern United States (SE-US) and for the North China Plain (NCP), which have been intensively investigated and discussed in earlier studies. As indicated in table S1, the SE-US scenario is characterized by relatively low aerosol concentration, low aerosol water content (AWC), and high temperature, as observed under clean-air summer conditions in the southeastern United States. By contrast, the NCP scenario is characterized by the high aerosol concentration, high AWC, and low temperature observed during extreme winter haze events in the Beijing region.

In aqueous solutions, the pH of different buffer systems is usually determined by the pK_a (where K_a is the acid dissociation constant) of the buffering agents (*26*). Accordingly, the different pH buffer levels in fig. S1 would suggest different buffering agents corresponding to different particle chemical compositions. To identify the most relevant buffering agents, key controlling parameters, we introduce the concept of a multiphase buffering capacity that describes the resistance to pH changes upon input of acids or bases in an aerosol multiphase system in analogy to the traditional buffering capacity of bulk aqueous solutions. The buffering capacity β is defined as the ratio between the amount of acid or base added to the system (n_{acid} or n_{base}, in moles per kilogram) and the corresponding pH change in the aqueous phase of the system, or $\beta = -dn_{acid}/d\mathrm{pH} = dn_{base}/d\mathrm{pH}$. The larger the buffering capacity β, the less the pH will change upon the addition of acids or bases.

Figure 1A shows the buffering capacities for the SE-US and NCP aerosol scenarios and for bulk aqueous solutions of the individual buffering agents (i.e., conjugate acid-base pairs NH_4^+/NH_3, HSO_4^-/SO_4^{2-}, and HNO_3/NO_3^-) as derived from numerical simulations of the gas-liquid and acid-base equilibria [see materials and methods, section M1; results of the northern India and western Europe scenarios are in fig. S2; and results of organic buffers are in the supplementary text, section S7 (*25*)]. In both aerosol scenarios, the largest buffering capacity is obtained for the acid-base pair NH_4^+/NH_3 followed by HSO_4^-/SO_4^{2-} and HNO_3/NO_3^-. The peak buffer pH value (defined as the pH corresponding to the highest local maximum of β) for the SE-US scenario is ~0.7, and the peak buffer pH value for the NCP scenario is ~4.5. Thus, the buffer pH ranges (i.e., peak buffer pH ± 1) (*26*, *27*) closely match the aerosol pH ranges previously reported for the southeastern United States and for Beijing, respectively. This indicates that the conjugate acid-base pair NH_4^+/NH_3 is the main buffering agent in both the SE-US and NCP aerosol scenarios.

This finding raises the question of how the same buffering agent can stabilize the aerosol pH at very different levels. As shown in Fig. 1A, in bulk aqueous solution, the peak buffer pH of NH_4^+/NH_3 is ~9.2, but in the NCP and SE-US aerosol scenarios, it shifts to much lower values of ~4.5 and ~0.7, respectively. By contrast, the peak buffer pH of the conjugate acid-base pair HNO_3/NO_3^- shifts in the opposite direction from ~−1.5 in the bulk aqueous solution to higher values of ~0.2 and ~3.8 in the NCP and SE-US scenarios, respectively. The conjugate acid-base pair HSO_4^-/SO_4^{2-}, on the other hand, exhibits similar peak buffer pH values of ~2 in all three scenarios (Fig. 1A). These differences and shifts of peak buffer pH reflect special features of the aerosol multiphase buffer system that go beyond the traditional buffer theory for bulk aqueous solutions, and they highlight the need for a mechanistic understanding of the multiphase buffering mechanism in atmospheric aerosols.

To elucidate the underlying mechanisms and key parameters, we have developed a multiphase buffer theory and derived an analytical expression for the buffering capacity of a buffering agent X (conjugate acid-base pair) in an aerosol multiphase buffer system as detailed in section S1 (*25*)

$$\beta = \frac{dn_{base}}{d\mathrm{pH}} = 2.303\left\{\frac{K_w}{[H^+]} + [H^+] + \sum_i \frac{K_{a,i}^*[H^+]}{(K_{a,i}^* + [H^+])^2}[X_i]_{tot}^*\right\} \quad (1)$$

[1]Minerva Research Group, Max Planck Institute for Chemistry, Mainz 55128, Germany. [2]Multiphase Chemistry Department, Max Planck Institute for Chemistry, Mainz 55128, Germany. [3]Scripps Institution of Oceanography, University of California, San Diego, La Jolla, CA 92093, USA. [4]Department of Geology and Geophysics, King Saud University, 11451 Riyadh, Saudi Arabia.
*Corresponding author. Email: yafang.cheng@mpic.de (Y.C.); h.su@mpic.de (H.S.)

Here, K_w is the water dissociation constant, $[X_i]_{tot}^*$ represents the total equivalent molality of the buffering agent X_i, including the gas phase and aqueous phase of both conjugate acid-base species—e.g., the sum of $NH_3(g)$, $NH_3(aq)$, and $NH_4^+(aq)$ for the buffering agent NH_4^+/NH_3. $K_{a,i}^*$ is an effective acid dissociation constant of the buffering agent X_i and can be expressed by

$$K_{a,BOH}^* = \frac{[H^+(aq)]\left([BOH(aq)] + [BOH(g)]\right)}{[B^+(aq)]} = K_{a,BOH}\left(1 + \frac{\rho_w}{H_i R T \, AWC}\right) \quad (2A)$$

$$K_{a,HA}^* = \frac{[H^+(aq)][A^-(aq)]}{[HA(aq)]+[HA(g)]} = K_{a,HA}/\left(1 + \frac{\rho_w}{H_i R T \, AWC}\right) \quad (2B)$$

for volatile base BOH and volatile acid HA that dissociate in the form

$$B^+(aq) + H_2O \rightleftharpoons H^+(aq) + BOH(aq) \quad (2C)$$

$$HA(aq) \rightleftharpoons H^+(aq) + A^-(aq) \quad (2D)$$

As shown in Eq. 2, the effective dissociation constant $K_{a,i}^*$ depends on the classical dissociation constant $K_{a,i}$ as well as on the Henry's law coefficient H_i (gas-particle partitioning constant) (in moles per liter per atmosphere) and on the AWC (in micrograms per cubic meter)—i.e., the amount of liquid water in the aerosol multiphase system. Here, ρ_w is the liquid water density (~10^{12} μg m^{-3}), R is the gas constant (8.205 ×10^{-2} atm L mol^{-1} K^{-1}), and T is the absolute temperature (in kelvin). Note that gas concentrations in square brackets are expressed in units of equivalent molality (in moles per kilogram of water) [see section M1 (*25*)]. The expression of Eqs. 1 and 2 in the other unit system can be found in section S2.

By solving Eq. 1, we can find a local maximum of β at pH = $pK_{a,i}^*$; i.e., the peak buffer pH of the agent X_i is determined by $K_{a,i}^*$. Therefore, a single buffering agent can have its peak buffering capacity at very different pH values in an aerosol multiphase buffer system. According to Eq. 2A, for the buffering agent NH_4^+/NH_3 (volatile base), increasing AWC results in a reduced K_a^* and increased pK_a^*. Thus, the traditional alkaline buffering agent NH_4^+/NH_3 effectively becomes an acidic buffering agent ($pK_a^* < 7$) in multiphase systems (Fig. 1A). For volatile acid buffering agents (HNO_3/NO_3^-), the AWC has the opposite effect on pK_a^* (Fig. 1A). Moreover, the shift of pK_a^* upon changes to the AWC is inversely proportional to the partitioning coefficient H_i. Thus, the volatile buffering agents HNO_3/NO_3^- and NH_4^+/NH_3 (low H_i) exhibit large shifts, whereas the peak buffer pH of HSO_4^-/SO_4^{2-} hardly changes (high H_i) (table S2). As shown in Fig. 1B, the effective dissociation constant K_a^* converges with the standard acid-base dissociation constant of the buffering agent for high values of AWC (Eq. 2), and the multiphase buffer theory converges with the conventional buffer theory in solution chemistry [see sections S1 to S4 (*25*)]. Note that activity coefficients must be considered in the calculation of nonideal systems [see section S3 (*25*)].

Figure 2 further explains the thermodynamics that causes the shift of buffer pH in a multiphase system. The conventional bulk buffer solutions (e.g., NH_4^+/NH_3), assuming no exchange with a gas phase, achieve their largest resistance to pH change when the molality of $NH_4^+(aq)$ is equal to that of $NH_3(aq)$ (Eq. 3A) (*26*)

$$pH = pK_{a,NH_3} + \log_{10}\frac{[NH_3(aq)]}{[NH_4^+(aq)]} \quad (3A)$$

where

$$K_{a,NH_3} = \frac{K_w}{K_{b,NH_3}} = \frac{[H^+(aq)][NH_3(aq)]}{[NH_4^+(aq)]} \quad (3B)$$

and K_{b,NH_3} is the base dissociation constant of NH_3 (table S2).

For gas-liquid multiphase systems, this equilibrium is extended to the gas phase, and pH becomes a function of K_a^* and the ratio of total NH_3 in both gas and aqueous phase to NH_4^+ in the aqueous phase [Eq. 4A; section S1 (*25*)]. Accordingly, the largest resistance to pH change under given $[NH_3]_{tot}^*$ ($[NH_3]_{tot}^*$ =$[NH_3(aq)]$ + $[NH_3(g)]$ + $[NH_4^+(aq)]$) is achieved when the molality of $NH_4^+(aq)$ is equal to the sum of $NH_3(aq)$ and $NH_3(g)$. Note that Eq. 3 still holds for the aqueous phase in the multiphase system

$$pH = pK_{a,NH_3}^* + \log_{10}\frac{[NH_3(aq)]+[NH_3(g)]}{[NH_4^+(aq)]} \quad (4A)$$

where

$$K_{a,NH_3}^* = \frac{[H^+(aq)]\left([NH_3(aq)]+[NH_3(g)]\right)}{[NH_4^+(aq)]} = K_{a,NH_3}\left(1 + \frac{\rho_w}{H_{NH_3} RT AWC}\right) \quad (4B)$$

Figure 2 shows the conditions where the peak buffer pH values are achieved in different systems—i.e., the same height of NH_4^+ and NH_3 in each panel represents their same molar numbers in each system. Compared with bulk

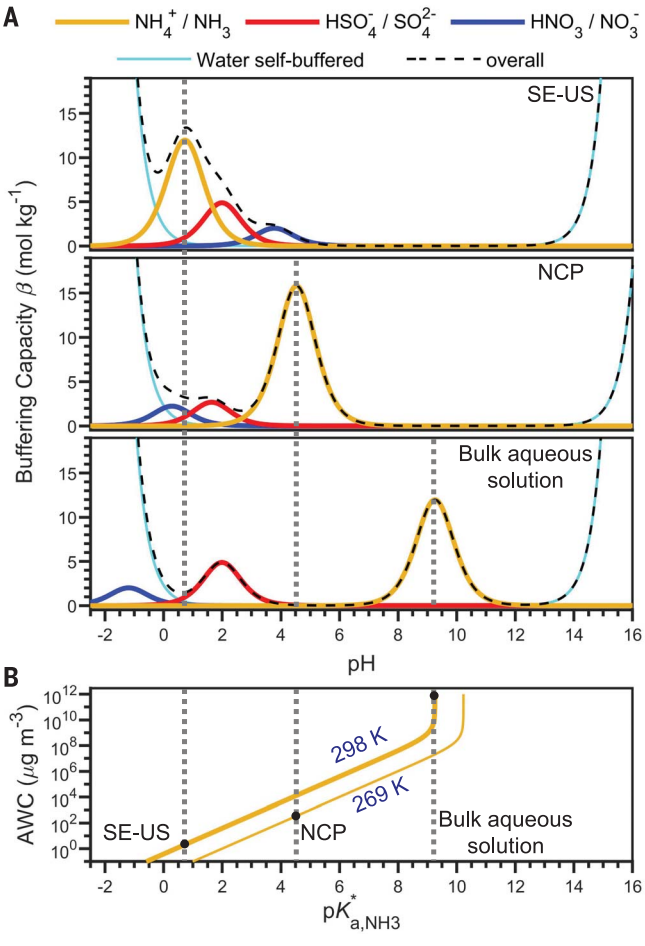

Fig. 1. Buffering capacity for aerosol multiphase systems compared with bulk aqueous solution. (**A**) Buffer capacities (β) for the SE-US and NCP aerosol scenarios and for bulk aqueous solution of individual buffering agents (solid lines). The overall buffering capacity (black dashed lines) is obtained by adding the individual buffer agent contributions to the solvent background of water [fig. S3 and section S5 (*25*)]. The composition of the bulk solution is assumed to have the same aqueous phase molality as in the SE-US scenario. (**B**) Dependence of the peak buffer capacity (pK_a^*) of NH_4^+/NH_3 on aerosol water content (AWC) and temperature.

solution, a fraction of NH_3 partitions to the gas phase in the NCP scenario, which results in less NH_3(aq) and a reduced [NH_3(aq)]/[NH_4^+(aq)] ratio, which leads to a lower pH in the aqueous phase according to Eq. 3. Further reduction of AWC in the SE-US scenario will push more NH_3 to the gas phase and further reduce the aerosol pH.

Figure 3 compares the contribution of individual factors in explaining the difference in aerosol pH between the NCP (~5.4) and SE-US (~0.7) scenarios in fig. S1 [sections M2, S3, S5, and S6 (*25*)]. The AWC appears to be the most important factor, contributing 2.2 units of pH change (ΔpH), followed by *T*, which contributes another 1.6 units of ΔpH. Although earlier studies have hypothesized that the marked observed pH difference is caused by a transition in particle chemical composition from a sulfate- to a nitrate-dominated regime (*12*, *19*), our results show that the change of chemical composition only plays a minor role. Different AWCs [mainly caused by different aerosol concentrations at a given relative humidity (RH)] and *T* values can already explain a shift of ~4 units of aerosol pH. The difference in chemical composition contributes ~0.7 pH units in total, with ~0.5 from the difference in total NH_3 fraction and ~0.1 and ~0.1 from the difference in the fraction of NO_3^- and nonvolatile cations (NVCs), respectively. Overall, different AWCs and *T* values are the main drivers of the pH difference between the NCP and SE-US scenarios, whereas the higher fraction of total NH_3, NVCs, and NO_3^- in the NCP further enlarges the difference.

In Fig. 4, we performed global model simulations to identify the buffered regions and used both simulation and observational data to further compare the roles of AWC and chemical compositions in determining the variabilities of aerosol pH [sections M3, S3, and S6 and table S3 (*25*)]. As shown in Fig. 4A, ~40% of continental surface areas (not including Antarctica) and 71% of urban populated areas were buffered by the NH_4^+/NH_3 agent with aerosol pH values mostly within the buffer range [$pK_{a,NH3}^* \pm 1$ (*26*, *27*)]. In these regions, without knowing the temporal and spatial variability of particle chemical composition, variations in AWC alone explain almost 70% (R^2 = 0.66, simulation; where R^2 is the coefficient of determination) and 80% (R^2 = 0.77, observation) of the variation of aerosol pH, assuming an NH_4^+/NH_3–buffered system (Fig. 4B). On the other hand, when a constant AWC is assumed, distinct variations of aerosol acidity with particle chemical composition were observed, but they only played a secondary role (R^2 = 0.22 and 0.26 for simulation and observation, respectively; Fig. 4C). We also found a reverse role for AWC and composition in regions that are not buffered by NH_4^+/NH_3, where chemical composition differences alone explain >90% of the variations of aerosol pH (fig. S5). Overall,

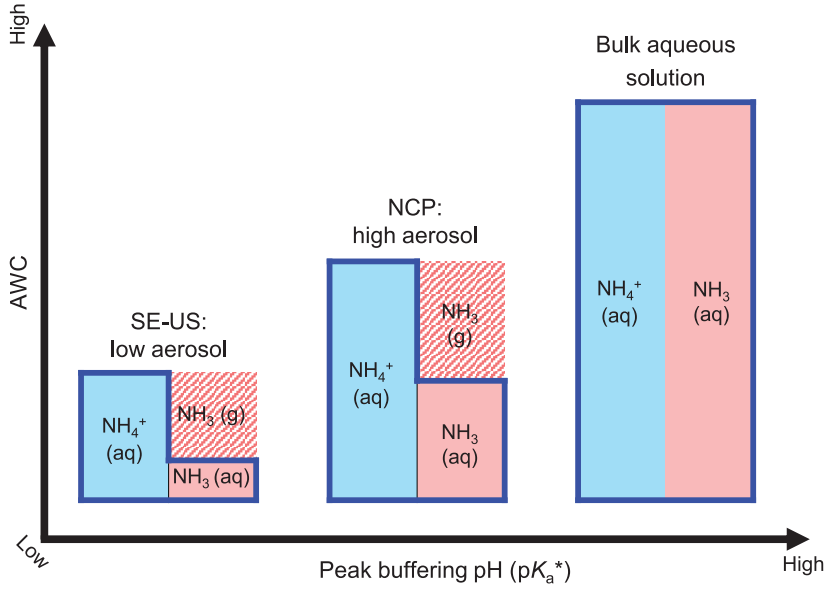

Fig. 2. Schematic diagram of buffer pH transition from aerosol multiphase systems to bulk aqueous solution for NH_4^+/NH_3. AWC concentrations are not drawn to scale, for illustration purposes. Diagrams for a generic volatile acid and base are shown in fig. S4.

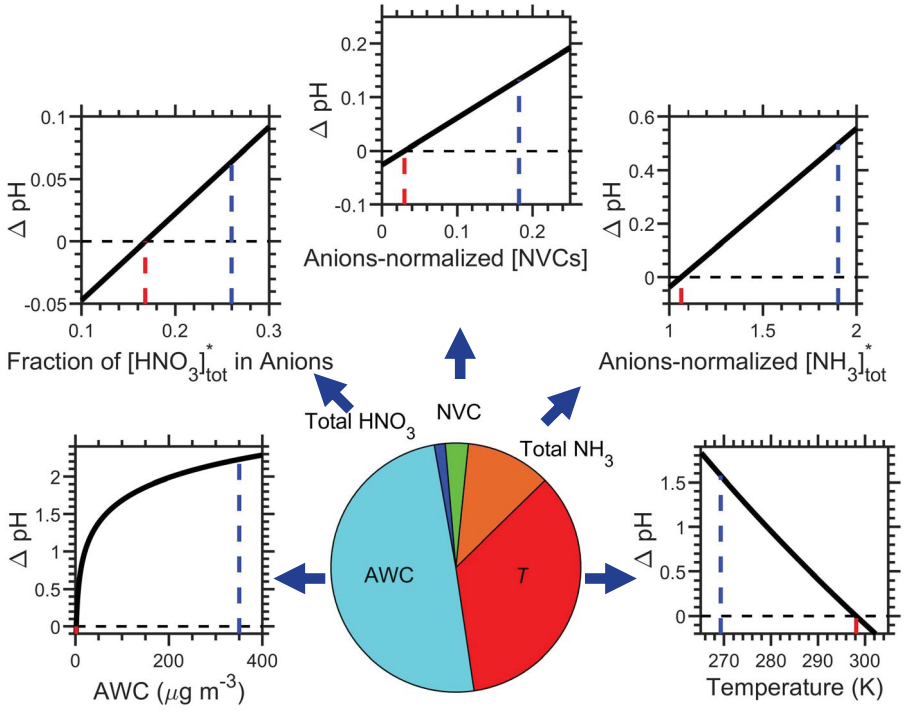

Fig. 3. Fractional contribution of individual drivers to the aerosol pH difference between SE-US and NCP scenarios. Red and blue lines mark the corresponding values in the SE-US and NCP scenarios, respectively [see table S1 for detailed scenario information (*25*)].

the buffering effect of ammonia suppresses the influence of compositional differences, making aerosol water content the primary determinant of aerosol pH.

The multiphase buffering of aerosols and the key role of AWC in determining the peak buffer pH (pK_a^*) have implications for atmospheric research and air pollution control. Drivers of historical trends in aerosol pH can now be better understood and quantified [section S8 (*25*)]. In populated continental regions with high anthropogenic emissions and atmospheric concentrations of ammonia (*28*), aerosol pH is likely controlled by the buffering pair NH_4^+/NH_3 and can thus be approximated on the basis of aerosol mass concentration and

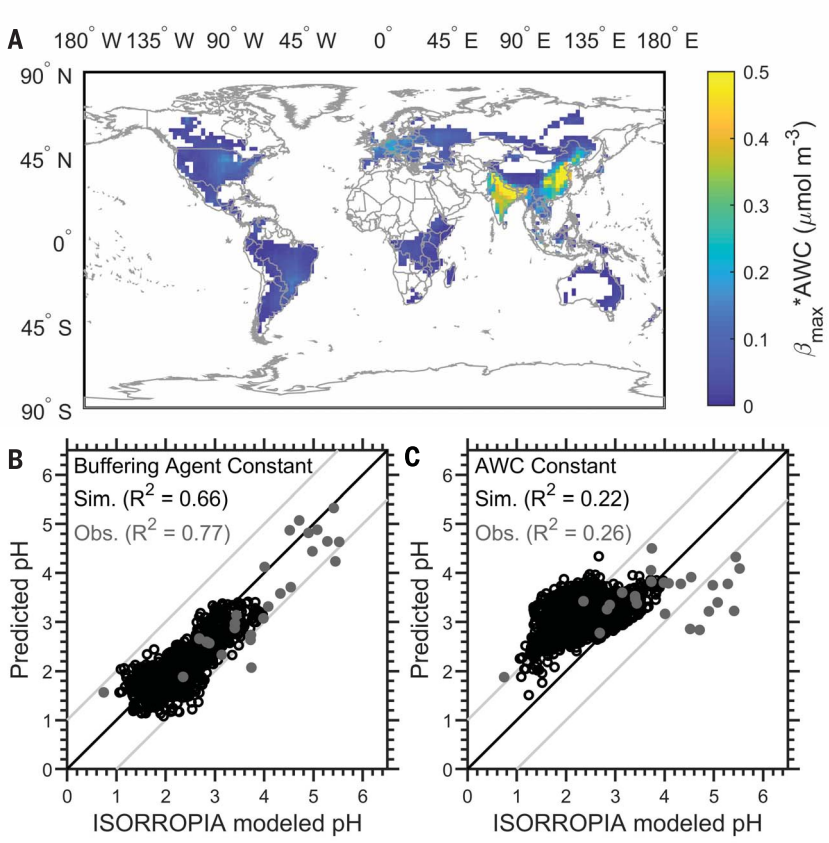

Fig. 4. Drivers of aerosol pH diversity in ammonia-buffered regions. (**A**) Global distribution of continental surface regions buffered by NH_4^+/NH_3. The color coding shows the maximum buffer capacity by NH_4^+/NH_3 (in moles per cubic meter of air). (**B**) Correlation of aerosol pH modeled by ISORROPIA with the predicted pH derived using constant buffering agent and multiphase buffer theory. Sim., simulation; Obs., observation. (**C**) Correlation of aerosol pH modeled by ISORROPIA with the predicted pH by ISORROPIA using constant AWC but variable compositions. Black circles and gray dots represent analysis based on model simulations and observations, respectively (see section M3 and table S3). Note that the observations are based on individual case studies and thus show a wider range of aerosol pH than the annual average simulation results.

water content (Eq. 4). This opens up possibilities to reconstruct long-term trends and large-scale spatial distributions of aerosol pH. Other buffering agents, such as HSO_4^-/SO_4^{2-}, HCl/Cl^-, or HCO_3^-/CO_3^{2-}, are likely to control aerosol pH over the oceans (*13*, *14*, *29*, *30*), but the buffering effects of NH_4^+/NH_3 may extend over ammonia-rich coastal and downwind regions. Thus, the notable human influence on ammonia emissions and the global nitrogen cycle in the Anthropocene substantially affects aerosol pH and atmospheric multiphase chemistry on a global scale.

REFERENCES AND NOTES

1. J. H. Seinfeld, S. N. Pandis, *Atmospheric Chemistry and Physics: From Air Pollution to Climate Change* (Wiley, 2016).
2. D. J. Jacob, J. W. Munger, J. M. Waldman, M. R. Hoffmann, *J. Geophys. Res. Atmos.* **91**, 1073–1088 (1986).
3. D. J. Jacob, J. M. Waldman, J. W. Munger, M. R. Hoffmann, *J. Geophys. Res. Atmos.* **91**, 1089–1096 (1986).
4. A. R. Ravishankara, *Science* **276**, 1058–1065 (1997).
5. M. Jang, N. M. Czoschke, S. Lee, R. M. Kamens, *Science* **298**, 814–817 (2002).
6. S. Gao *et al.*, *Environ. Sci. Technol.* **38**, 6582–6589 (2004).
7. J. D. Surratt *et al.*, *Environ. Sci. Technol.* **41**, 5363–5369 (2007).
8. Y. Cheng *et al.*, *Sci. Adv.* **2**, e1601530 (2016).
9. D. W. Dockery *et al.*, *Environ. Health Perspect.* **104**, 500–505 (1996).
10. W. Li *et al.*, *Sci. Adv.* **3**, e1601749 (2017).
11. E. Harris *et al.*, *Science* **340**, 727–730 (2013).
12. H. O. T. Pye *et al.*, *Atmos. Chem. Phys.* **20**, 4809–4888 (2020).
13. W. C. Keene, A. A. P. Pszenny, J. R. Maben, R. Sander, *Geophys. Res. Lett.* **29**, 1101 (2002).
14. B. Alexander *et al.*, *J. Geophys. Res. Atmos.* **110**, D10307 (2005).
15. R. J. Weber, H. Guo, A. G. Russell, A. Nenes, *Nat. Geosci.* **9**, 282–285 (2016).
16. M. Liu *et al.*, *Geophys. Res. Lett.* **44**, 5213–5221 (2017).
17. G. Shi *et al.*, *Environ. Sci. Technol.* **51**, 4289–4296 (2017).
18. S. Song *et al.*, *Atmos. Chem. Phys.* **18**, 7423–7438 (2018).
19. H. Guo, R. J. Weber, A. Nenes, *Sci. Rep.* **7**, 12109 (2017).
20. C. Fountoukis, A. Nenes, *Atmos. Chem. Phys.* **7**, 4639–4659 (2007).
21. H. Guo *et al.*, *Atmos. Chem. Phys.* **15**, 5211–5228 (2015).
22. G. J. Zheng *et al.*, *Atmos. Chem. Phys.* **15**, 2969–2983 (2015).
23. S. N. Behera, M. Sharma, *Sci. Total Environ.* **408**, 3569–3575 (2010).
24. L. Bencs *et al.*, *J. Environ. Monit.* **10**, 1148–1157 (2008).
25. See supplementary materials.
26. P. Atkins, L. Jones, *Chemical Principles: The Quest for Insight* (Macmillan, 2007).
27. H. N. Po, N. Senozan, *J. Chem. Educ.* **78**, 1499 (2001).
28. M. Van Damme *et al.*, *Nature* **564**, 99–103 (2018).
29. W. C. Keene, D. L. Savoie, *Geophys. Res. Lett.* **25**, 2181–2184 (1998).
30. D. J. Gaspar, A. Laskin, W. Wang, S. W. Hunt, B. J. Finlayson-Pitts, *Appl. Surf. Sci.* **231-232**, 520–523 (2004).

ACKNOWLEDGMENTS

Funding: This study is support by the Max Planck Society (MPG). Y.C. thanks the Minerva Program of MPG. **Author contributions:** Y.C. and H.S. conceived the theory and led the study. G.Z., Y.C., and H.S. performed the research. S.W. performed the GEOS-Chem simulation. M.O.A. commented on the manuscript. H.S., Y.C., G.Z., and U.P. wrote the manuscript with inputs from all coauthors. **Competing interests:** The authors declare no competing interests. **Data and materials availability:** All data used in the analysis are provided in the supplementary materials.

SUPPLEMENTARY MATERIALS

science.sciencemag.org/content/369/6509/1374/suppl/DC1
Materials and Methods
Supplementary Text
Figs. S1 to S15
Table S1 to S4
References (*31*–*97*)
Data S1

29 November 2019; accepted 21 July 2020
10.1126/science.aba3719

Multiphase buffer theory explains contrasts in atmospheric aerosol acidity

Guangjie Zheng, Hang Su, Siwen Wang, Meinrat O. Andreae, Ulrich Pöschl and Yafang Cheng

Science **369** (6509), 1374-1377.
DOI: 10.1126/science.aba3719

A multiphasic effect

Aerosols exert a primary influence on atmospheric chemistry. One of the main controls on their internal chemistry is their acidity, so understanding what determines aerosol pH is fundamental for determining their environmental effects. Zheng *et al.* considered how buffering capacity in a multiphase aerosol system differs from bulk solution and found an important role for water content in determining pH in ammonia-buffered regions. Their conclusions underscore the important influence of ammonia emissions in the Anthropocene.

Science, this issue p. 1374